PAPER • OPEN ACCESS

Improved analysis and visualization of friction loop data: unraveling the energy dissipation of meso-scale stick–slip motion

To cite this article: Jaap Kokorian and W Merlijn van Spengen 2017 *Meas. Sci. Technol.* **28** 115011

View the article online for updates and enhancements.

You may also like

- Excitation of energy harvesters using stick–slip motion
  L E Helseth

- Confined cubic blue phases under shear
  O Henrich, K Stratford, D Marenduzzo et al.

- Effects of stick–slip motions on Besocke-style scanners in scanning probe microscopes
  Hui Zhang, Shu-yi Zhang and Li Fan

Corrigendum

Corrigendum: Improved analysis and visualization of friction loop data: unraveling the energy dissipation of meso-scale stick–slip motion (2017 *Meas. Sci. Technol.* **28 115011**)

Jaap Kokorian[1,2] and W Merlijn van Spengen[1,3]

[1] TU Delft, 3mE-PME-MNE, Mekelweg 2, 2628 CD, Delft, The Netherlands
[2] Philips Medical Systems International B.V. Veenpluis 4-6, 5684 PC Best, The Netherlands
[3] Falco Systems B.V., Van Boshuizenstraat 12, 1083 BA, Amsterdam, The Netherlands

E-mail: jkokorian@gmail.com

CrossMark

In this corrigendum we point out a mathematical error in our manuscript and review the consequences. None of the conclusions of the paper were impacted by the mistake. However, the original calculation and interpretation of the dynamically dissipated energy was incorrect. This resulted in two misleading figures, of which we include the corrected versions here.

1. Introduction

In our original manuscript [1], we introduced a new type of friction loop, in which the lateral (friction) force was plotted as against the x-position of the contact point on the sliding surface, instead of an equivalent of the cantilever support position of a friction force microscope (FFM). These loops are more intuitive than traditional FFM-style friction loops. They consist of continuous sections of dry friction, that are connected by 'data-less' gaps, where the coulomb limit is exceeded and the contact moves to the next stick location, faster than we can measure. In contrast to the FFM-style friction loops, the surface area of the new loops does not directly represent the dissipated energy: only the surface area below

the continuous parts really represents dissipated energy. We called this energy semi-statically dissipated energy. No surface exists in the gaps between the stick locations, so the dissipated energy during these sliding motions cannot be found by numerical integration.

2. Mistakes

In the original paper we correctly stated that despite the absence of data during the slip motions, we still know how much energy is dissipated. The amount of energy stored in the mechanical springs just before the slip occurs, minus the potential energy in the springs after the slip occurred, must be equal exactly to the amount of energy dissipated during the slip motion, because of the law of conservation of energy. Potential energy is stored in the spring, it starts to slip, potential energy is converted to kinetic energy, after a while the contact gets stuck and the remaining kinetic energy is converted to heat.

We explained that the dynamically dissipated energy equals the surface area of the triangles below the slip arrows (see figure 1(a)), excluding the remaining rectangle area between this triangle and the x axis. This claimed was backed up by an incorrect mathematical equation with a subtly hidden mistake: $(a + b)^2 \neq a^2 + b^2$. Because we forgot about the factor $2ab$, we simplified the equation more than possible (equations (20) and (21) in [1]).
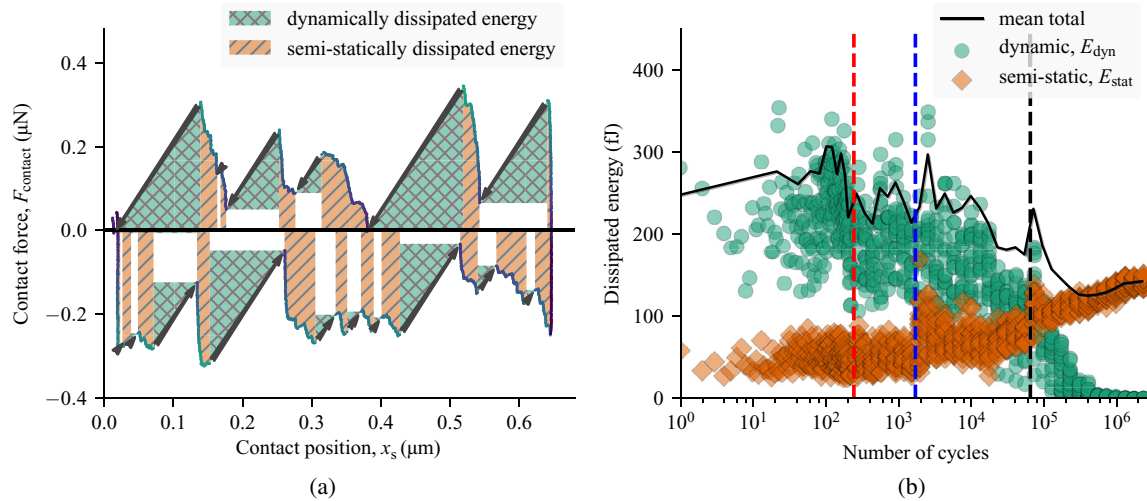
Figure 1. The original figure. The friction loop in figure (a) incorrectly shows green shaded areas to represent the dynamically dissipated energy. The evolution of the dissipated energy in figure (b) incorrectly shows that the dynamically dissipated energy decreases to zero after many sliding cycles.
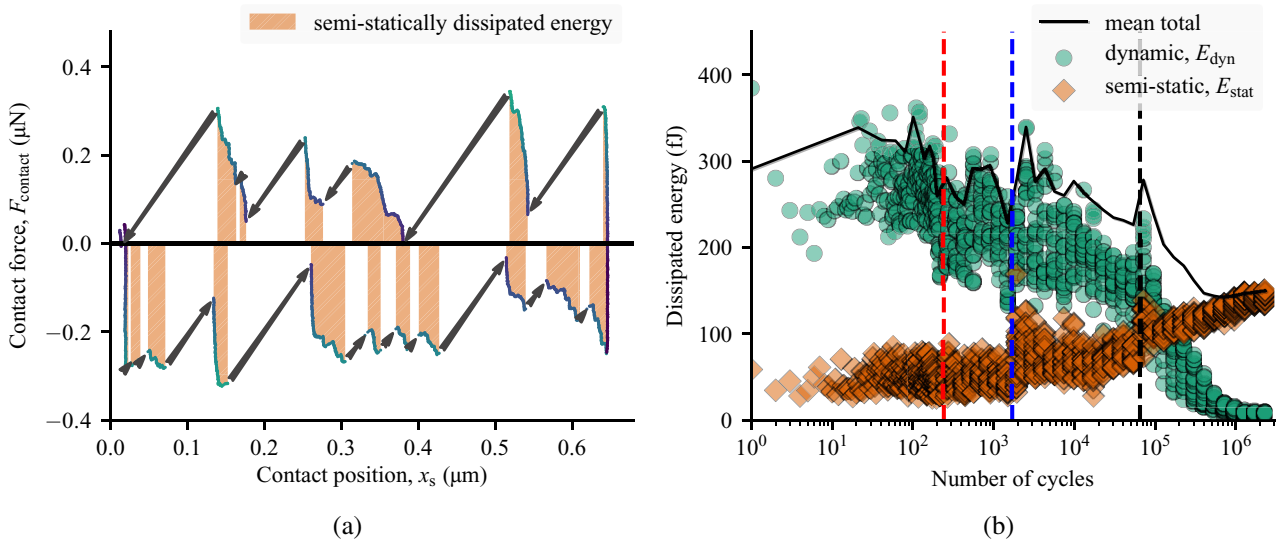
Figure 2. Corrected figure. In figure (a), the dynamically dissipated energy is no longer displayed in the friction loop as a shaded area, because it does not correspond to a surface area on these axes. In figure (b), the dynamically dissipated energy does not approach true zero, but a small value close to zero instead.

3. Corrections and conclusion

Fortunately, none of the main conclusions of the original manuscript depend on the incorrect math. However, the error did result in an incorrect shaded visualization of the dynamically dissipated energy in figure 1(a). A corrected version is shown in figure 2(a). We have chosen to omit the shading of the dynamic friction parts of the friction loop (the arrows) entirely, because the dynamically dissipated energy does not correspond to an area of the graph in a sensible way.

The exact values of the dynamically dissipated energy plotted against the number of sliding cycles in figure 1(b) also change, but only subtly. The corrected version is shown in figure 2(b). Most notably, the dynamically dissipated energy does not actually go to zero, but approaches a value very close to zero instead.

Acknowledgments

ORCID iDs

Jaap Kokorian https://orcid.org/0000-0001-9147-5869

Reference

[1] Kokorian J and van Spengen W M 2017 Improved analysis and visualization of friction loop data: unraveling the energy dissipation of meso-scale stick–slip motion *Meas. Sci. Technol.* **28** 115011

Improved analysis and visualization of friction loop data: unraveling the energy dissipation of meso-scale stick–slip motion

Jaap Kokorian[1,2] **and W Merlijn van Spengen**[1,3]

1 TU Delft, 3mE-PME-MNE, Mekelweg 2, 2628 CD, Delft, Netherlands
2 Philips Medical Systems Nederland B.V., Veenpluis 4-6, 5684 PC Best, Netherlands
3 Falco Systems B.V., Van Boshuizenstraat 12, 1083 BA, Amsterdam, Netherlands

E-mail: J.Kokorian@TUDelft.nl

Abstract

In this paper we demonstrate a new method for analyzing and visualizing friction force measurements of meso-scale stick–slip motion, and introduce a method for extracting two separate dissipative energy components. Using a microelectromechanical system tribometer, we execute 2 million reciprocating sliding cycles, during which we measure the static friction force with a resolution of 0.6 nN and the displacement with a resolution of 0.2 nm. We plot the lateral force as a function of the real contact position by compensating for the values of the spring constants of the system. This allows all friction loops to be combined in a single hexagonal bin plot, which clearly shows the evolution of the friction force magnitude and its distribution across the sliding track. We identify all individual slip events in the entire experiment using a thresholding algorithm. This allows us to show the evolution of the slip event count, the static friction force, and the coefficient of friction. Crucially, it allows us to disentangle the dissipated energy into two components: the dynamically dissipated energy, which is associated with slip motions, and the semi-statically dissipated energy, which is related to small contact deformations, plastic yield and other non-elastic behavior. Our technique provides new insight into the mechanics of stick–slip motion in multi-asperity contact systems, and paves the way towards a better understanding of the physics of meso-scale friction.

Keywords: microelectromechanical systems, MEMS tribometer, step detection, high resolution displacement measurement, high resolution friction force measurement, energy dissipation, friction

S Supplementary material for this article is available online

(Some figures may appear in colour only in the online journal)

1. Introduction

The field of macro-scale tribology—the study of friction, wear, and lubrication—has long since been occupied with the acquisition of tabular data on lubricants, friction coefficients and wear rates, under a large number of circumstances. This is extremely valuable information when designing a macro-scale mechanical system like an engine, or a Mars rover. There are phenomenological models [1–5] which predict the behavior of macro-scale friction forces to a certain extent, but still no physical models exist that are capable of predicting the tabulated values from first principles.

At the atomic scale, the bottom end of the size spectrum, the situation is rather different. Great advances have been made in our understanding of atomic scale friction due to the invention of the friction force microscope (FFM), which has

led to the discovery of phenomena like atomic stick–slip [6], superlubricity [7, 8], and substrate-induced ice formation at room temperature [9]. The Prandtl–Tomlinson model [10] predicts the tip motion of an FFM with reasonable accuracy. This is possible because an FFM has only a single point of contact, or asperity, whereas in a macro-scale system the total number of asperities approaches infinity.

Unfortunately, neither the wealth of empirical data available for the macro-scale nor the 'simplicity' of the atomic scale directly solves the challenges that arise when operating somewhere in between these scale regimes: at the meso-scale. At this scale, the contact area of two touching components is typically of the same order of magnitude as the surface roughness features, which means that the contact mechanics can differ greatly from place to place on the very same surface [11]. Tabulating generic empirical data for engineering purposes is therefore nearly impossible. Because the number of asperities is larger than one but too small to be considered infinite, both the analytical and empirical models are invalid at the meso-scale.

The primary man-made occupants of the meso-scale are microelectromechanical systems (MEMS): tiny mechanical devices, fabricated using the same processes that are used for producing microelectronics. Many MEMS devices have found their ways into our daily lives, such as airbag sensors, the inertial sensors and microphones of smartphones, and inkjet printer heads. However, because of the small size of these devices, the surface-to-volume ratio of their moving components is much larger than in a macro-scale system. This causes surface interaction forces to dominate most other forces in the system. MEMS devices that rely on touching or sliding components for their operation are therefore highly unreliable. The MEMS community has dealt with this fact mostly by designing and fabricating only devices without sliding components.

Important steps have already been taken towards a solution. Self-assembled monolayers [12, 13], hard coatings [14], and especially vapor-phase lubrication [15] have been shown to work well for silicon MEMS devices, and hard materials like silicon carbide [16] and diamond [17] have been used as a replacement for silicon as the devices' structural material.

Despite these practical advances, however, our understanding of the physical processes that govern the contact mechanics in MEMS is still in a poor state. This is in part because it is still difficult to measure contact forces in MEMS with a high resolution.

Friction measurements in MEMS are usually performed using MEMS tribometers [18–20]. These are MEMS devices which have been built specifically to measure friction forces between two contacting surfaces of the tribometer itself. Friction forces are usually determined indirectly from the measured displacements of the sliding components of the tribometer. Many types of tribometers exist today, enabling friction and wear measurements under many different circumstances.

The data that results from micro-scale friction measurements is highly stochastic in nature. Details in the measurement data often correspond to singular events that may or may not occur by chance. The data is therefore often shown either
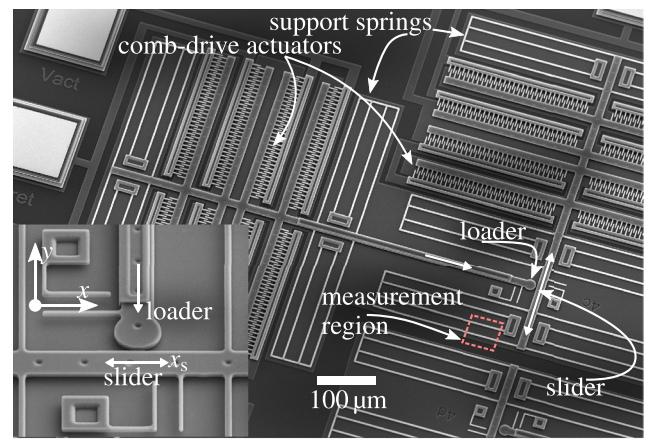
Figure 1. Scanning electron microscope (SEM) micrograph of the MEMS tribometer used in this study. The inset shows a close-up of the loader and the sliding slider. The red-dashed rectangle indicates the area on which the optical microscope was focused to track the position of the slider, x_s.

in its raw form, in order to show and discuss these details, or condensed into a single metric like the coefficient-of-friction, to compare the measurement to others quantitatively.

In this paper we show a new method for analyzing and visualizing the statistics of stick–slip friction and the evolution of the friction force. As a demonstration, we measure the evolution of the friction force between two sidewalls of a polycrystalline silicon MEMS tribometer with nanonewton resolution during millions of sliding cycles. We will present the measurement data in the form of a new type of friction loop, and with a hexagonal bin plot that represents all 2 million data points in a single graph. By automatically detecting slip events, we are able to chart the statistics of the stick–slip behavior, extract the maximum static friction force at each contact position and calculate the variability of the static friction force within a single loop. An important result of the new data analysis method is that we are able to determine the real amount of energy dissipation, which turns out to be split into two different contributions: a semi-static contribution, relating to non-stick–slip sliding and pre-sliding tangential deflections [21], and a dynamic contribution, relating to the dissipation of inertial forces during slip motions.

2. Experiments

The friction experiments were performed with a MEMS tribometer, as shown in figure 1. The design is based on the Leiden MEMS tribometer [20], and it was fabricated in the commercial PolyMUMPS multi-user fabrication process by MEMSCAP Inc. It consists of a normal loader, called the loader, and a sliding slider. Both the loader and the slider are suspended by folded flexure support springs which act as parallel guides. Each can be moved by a separate electrostatic comb-drive actuator [22]. Friction between the sidewalls of the loader and the slider is generated by moving the slider back and forth while pushing the loader against it. This is depicted schematically in figure 2. The important mechanical characteristics of the tribometer have been summarized in table 1.
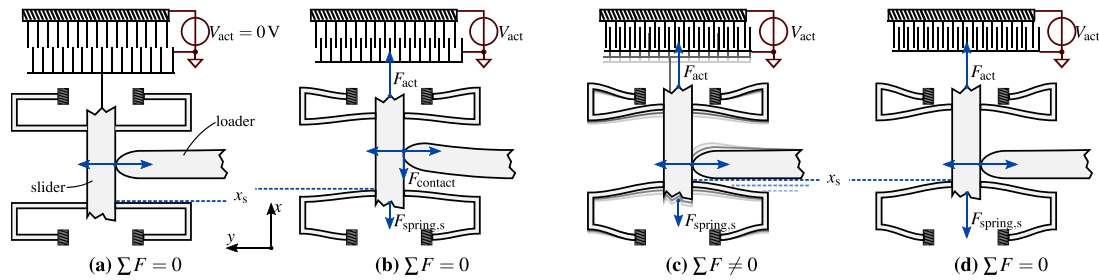
Figure 2. Operation principle of the MEMS tribometer shown in figure 1, during the measurement of stick–slip friction (image not to scale, displacements are exaggerated). The blue arrows indicate the forces acting on the slider. The position of the slider is given by x_s. (a) Equilibrium, no lateral contact force. (b) The comb drive actuator generates a force that pulls on the slider to which the loader is currently stuck. (c) The lateral contact force keeping the loader stuck to the slider exceeds the maximum friction force. The loader slips back to its neutral position and the slider moves to a new equilibrium position. (d) New equilibrium position, no lateral contact force.

The device was placed in an environmental chamber, inside which the atmosphere was kept at a temperature of $25 \pm 5\,°C$ and the relative humidity was kept below 5%. The chamber was fitted with a glass viewport to allow optical access to a Motic PSM-1000 optical microscope mounted above it. The friction sensor was illuminated through the microscope objective by a liquid light-guide-coupled Sutter HPX-L5 90W LED light source, which has the equivalent light output of a 150W xenon arc lamp. Images were captured by an IDS uEye 3370CP CMOS camera, mounted on top of the microscope. The entire setup was suspended in bungee cords inside an acoustic isolation booth mounted on active pneumatic supports in order to isolate the device from external mechanical and acoustical disturbances.

Throughout the entire experiment, a voltage of 85.0 V was applied to the comb-drive actuators of the loader, which pushed the loader against the slider with a force of 669 ± 51 nN. This force was determined from the voltage–displacement relationship of the loader using the method explained in our previous work on adhesion measurements [25]. Note that the normal force value given here refers only to the externally applied force. Because of adhesion, the actual normal force at that contact is somewhat higher and varies during the experiment.

In order to measure the friction force during a single reciprocating sliding motion, the actuator voltage of the slider actuator was increased from range 0V to 60V in 1000 steps and back again, while an optical microscope image of the moving slider and a fixed reference was captured at each step. The voltage step size decreases with the square-root of the voltage, to compensate for the quadratic relation between the actuator voltage and the displacement of the slider. This way, the slider moved from 0nm to 740nm and back in 2000 equal steps of 0.74nm. Measuring a single cycle this way takes 36 s. The position of the slider relative to the substrate was determined from the captured images at each voltage step with a resolution of 0.2 nm, using our in-house developed curve-fitting technique [26].

The entire experiment consisted of two parts. First, 200 consecutive sliding cycles were recorded in order to observe how the pristine surface changes during the first few cycles at a low velocity. Second, the sliding cycles were recorded in blocks of 20 consecutive cycles, in between which an exponentially increasing number of sliding cycles was performed

Table 1. Summary of the geometrical and mechanical properties of the MEMS tribometer shown in figure 1. The spring constants were calculated analytically using standard cantilever beam approximations [23]. The sidewall roughness was obtained from an AFM measurement by van Spengen *et al* [24], on a device that was fabricated using the same technology.

| Tribometer property	Value
Suspended structure thickness	$2.0\,\mu m$
Loader tip radius	$10.0\,\mu m$
Young's modulus of poly-silicon	158 ± 10 GPa
Loader suspension spring constant, $k_{y,L}$	2.6 ± 0.2 Nm^{-1}
Slider suspension spring constant, k_s	3.9 ± 0.2 Nm^{-1}
Sidewall RMS surface roughness [24]	13 ± 3 nm

at an average velocity of 50 μm s^{-1}. The total number of sliding cycles was 2 249 827.

3. Results

The resulting dataset consists of 1000 sliding cycles of 2000 measurement records each. Each record contains the voltage applied to the slider comb-drive actuators, and the measured slider displacement x_s relative to the substrate. In section 3.1, we show how to transform these raw values into the lateral force at the contact, $F_{contact}$, and the position at which the loader touches the slider, $x_{contact}$. We then study the evolution of the friction force and its distribution across the sliding track qualitatively: by analyzing the individual friction loops in section 3.2, and by introducing a new visualization method that displays many aspects of all recorded friction loops in a single plot in section 3.3. In section 3.4 we show how to identify individual slip events and we discuss their statistics. Finally, in section 3.5 we use this information to distinguish between two types of friction energy.

3.1. Calculation of the force and contact position from the raw data

Figure 3(a) shows an example of a single measured friction cycle in its rawest form: the measured slider position x_s versus the applied actuator voltage. The dashed-red line indicates the 'undisturbed motion' $x_{s,und}$: the displacement of the slider
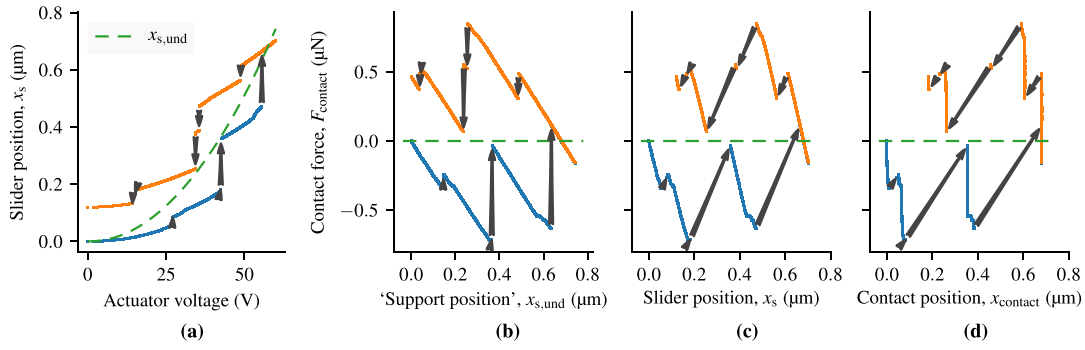
Figure 3. Transformation of the raw displacement measurement data, (a) to an FFM-style friction loop, (b) to a MEMS-style friction loop, (c) to a 'physical' friction loop (d). The arrows indicate slip motions. The slopes of the stick-parts of the friction loops in (b) and (c) depend on the spring constants of the measurement system, and correct interpretation of their horizontal axes requires knowledge of the measurement system components, which makes them less intuitive to interpret than the friction loop in (d).

when it is not in contact with the loader. The blue data points correspond to the measured slider positions during the forward sliding motion, and the orange data points correspond to the measurement slider positions during the backward sliding motion. At the continuous parts of the lines, the slider is stuck to the loader. The reason that stick-sections are not perfectly horizontal is that the slider can still move while being stuck, due to the finite bending stiffness of the loader. The arrows connecting the discontinuities indicate slip events. These are too fast for our measurement system to capture. The data points and the arrows together constitute a hysteresis loop, commonly referred to as 'friction loop'. Because the force of friction always acts in the direction opposite to the motion of the slider, $x_s \leqslant x_{s,und}$ during the forward motion, and $x_s \geqslant x_{s,und}$ during the backward motion.

To transform the voltage–displacement curve of figure 3(a) to a force–displacement curve, we first need to obtain a mathematical relationship between the measured displacement x_s, the actuator voltage V_{act} and the contact force $F_{contact}$. A schematic representation of the operation of the tribometer is shown in figure 2. The blue arrows indicate the forces acting on the slider. The force balance of all forces acting in the x-direction (the vertical direction in figure 2) is given by

$$\Sigma F_x = -F_{act} + F_{contact} + F_{spring,s} = m \cdot \frac{\mathrm{d}^2 x}{\mathrm{d}t^2}, \qquad (1)$$

where F_{act} is the force exerted by the slider's actuator comb drives, $F_{contact}$ is the contact exerted on the slider by the loader, and $F_{spring,s}$ is the restoring spring force of the slider support springs.

When the device is at rest, $\frac{\mathrm{d}^2 x}{\mathrm{d}t^2} = 0$, so we can write for the actuator force F_{act}:

$$F_{act} = F_{contact} + F_{spring,s} \qquad (2)$$

$$= F_{contact} + k_s \cdot x_s, \qquad (3)$$

where k_s is the spring constant of the slider support springs.

We do not actually have to know the value of F_{act} to obtain $F_{contact}$. Instead, we can calculate $F_{contact}$ for every value of V_{act} from the difference between the actual displacement of the slider x_s and the undisturbed displacement of the slider, $x_{s,und}$. When $F_{contact} = 0$, $x_s = x_{s,und}$ by definition. So:
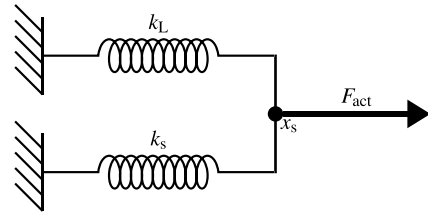
Figure 4. Mechanical lumped element model of the slider and loader of the MEMS tribometer shown in figure 1. It shows the equivalent lateral springs constants and forces acting on the slider while the loader is stuck to the slider due to static friction. This model corresponds to the state of the tribometer as shown in figure 2(b). When the loader is stuck against the slider, it acts as an additional spring in parallel to the folded flexure suspension.

$$F_{act} = k_s \cdot x_{s,und} \qquad \text{for } F_{contact} = 0. \qquad (4)$$

substitute (3) for F_{act}:

$$k_s \cdot x_s + F_{contact} = k_s \cdot x_{s,und} \qquad (5)$$

rearrange the terms:

$$F_{contact} = k_s \cdot (x_{s,und} - x_s). \qquad (6)$$

We use equation (6) to calculate the contact force from our measured values of x_s.

In AFM-based friction force microscopy, the contact force is usually plotted versus the cantilever support position. This quantity is very similar to our 'undisturbed motion' and can be explained using exactly the same wording as used above: it represents the position at which the cantilever tip would have been if the contact force had been zero. Because friction force microscopy is older than MEMS tribology, MEMS friction loops are often plotted the FFM way, which is shown in figure 3(b). The slope of the stick-parts of the plot depends on the spring constants of the system. Figure 4 shows a mechanical lumped element model that describes a situation in which the loader is stuck to the slider for $F_{act} \neq 0$ (figure 2(b)). From the lumped element model we know the relation between the slider displacement, x_s, the actuator force, F_{act}, the spring constant of the slider's support springs, k_s, and the spring constant that corresponds to the lateral bending mode of the loader, k_L:
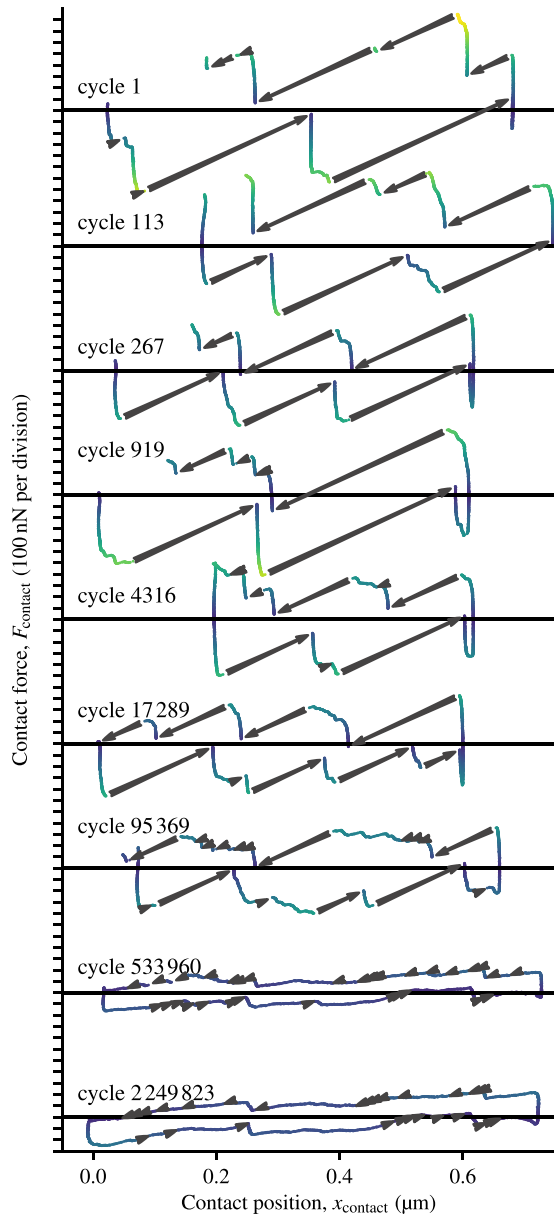
Figure 5. A number of friction loops recorded after an increasing number of contact cycles (first cycle on top). The arrows indicate slip motion events. The friction loops are displayed by plotting the lateral force versus the contact position $x_{contact}$. The color of the data points is proportional to the magnitude of the friction force and corresponds to the color scale used in figure 6.

$$x_s = F_{act} \cdot \frac{1}{k_L + k_s}. \tag{7}$$

Substitute (4) for F_{act}, and (6) for x_s:

$$x_{s,und} - \frac{F_{contact}}{k_s} \equiv x_{s,und} \cdot \frac{k_s}{k_L + k_s} \tag{8}$$

rearrange the terms:

$$F_{contact} \equiv x_{s,und} \cdot \frac{k_L \cdot k_s}{k_L + k_s} \tag{9}$$

finally differentiate with respect to $x_{s,und}$:

$$\frac{\partial F_{contact}}{\partial x_{s,und}} = \frac{k_L \cdot k_s}{k_L + k_s}. \tag{10}$$

This means that the shape of the friction loops depends strongly on the geometry of the measurement system, which makes them hard to interpret.

A more 'pure' way of plotting MEMS friction loops would be to place the measured slider position x_s on the horizontal axis, as is shown in figure 3(c). The slope of the stick-parts of the plot now only depends on k_L, which we can prove by substituting (3) for F_{act} in (7):

$$x_s = (F_{contact} + k_s \cdot x_s) \cdot \frac{1}{k_L + k_s} \tag{11}$$

simplifying:

$$F_{contact} = x_s \cdot (k_L + \cancel{k_s}) - \cancel{k_s \cdot x_s} \tag{12}$$

and differentiating with respect to x_s:

$$\frac{\partial F_{contact}}{\partial x_s} = k_L. \tag{13}$$

This means that k_L can now be calculated from the linear slopes of the friction loops, which allows for a third type of friction loop to be plotted: the force versus the actual contact position $x_{contact}$, where $x_{contact}$ is calculated from x_s and k_L using

$$x_{contact} = x_s - \frac{F_{contact}}{k_L}. \tag{14}$$

This type of friction loop is shown in figure 3(d). We will use it throughout the rest of this paper because it offers several important advantages over an FFM-style friction loop. First, its interpretation requires no knowledge of the geometry and components of the measurement system. Second, and more importantly, the surface area under any continuous section of the graph directly corresponds to the energy that was dissipated at that specific contact range. In an FFM-style friction loop, on the other hand, the surface area under any section of the graph corresponds to the potential energy stored in or gained from the support springs. Although it is possible to extract the dissipated energy at every contact position from an FFM-style loop indirectly, doing so is much less intuitive.
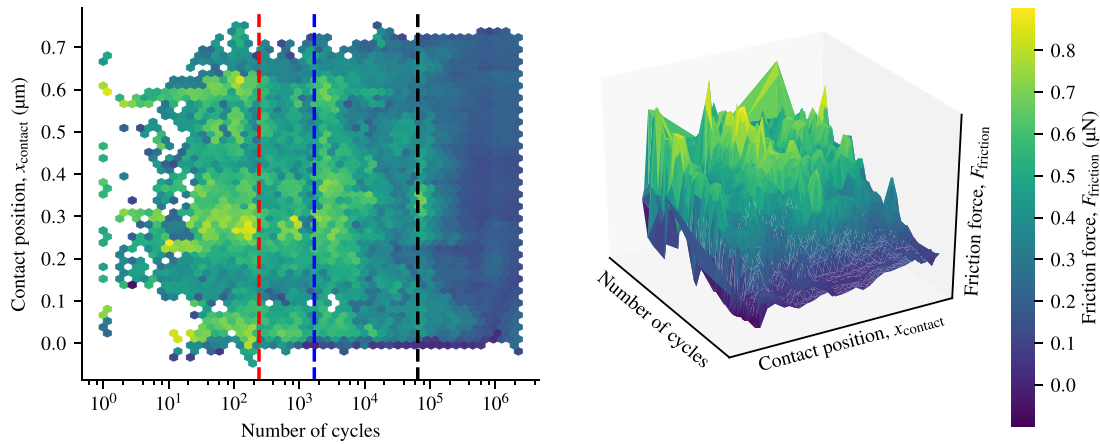
3.2. Raw friction loops

Several measured friction loops of the experiment are shown in figure 5. A movie of all individual friction loops can be found in the supplementary material (stacks.iop.org/MST/28/115011/mmedia). As promised, we have plotted the lateral contact force $F_{contact}$ on the vertical axis versus the contact position $x_{contact}$ on the horizontal axis.

Stick–slip motion measurements, such as this one, produce friction loops that consist of two contributions: continuous 'stick parts', where the slider is stuck to the loader, and discontinuous 'slip parts', where the slider slips.

Blue arrows are drawn between the start and end points of slip events. A slip event occurs when the actuator force F_{act}

Figure 6. Hexagonal bin plot of the maximum friction force measured at every contact position of all friction loops. The color of each bin corresponds to the maximum value of F_{friction}. The 3D surface plot has been constructed from the bin values and positions. We have used Matplotlib's [27] perceptually uniform colormap 'viridis'.

becomes greater than the static friction force, the contact is broken, and the slider moves to a new position where it gets stuck. Note that we do not have any measurements while the slider is slipping, because our measurement method is too slow to capture the slider while it is in motion. At every measurement point, the slider is stationary.

During the first few cycles, the slider is stuck most of the time. As more cycles elapse, the friction force decreases slightly, and a higher number of slip events occur. After 2 million cycles, the surface has become smooth, and the friction loops are almost continuous.

3.3. Hexagonal bin plots

Studying graphical representations of all 2000 recorded friction loops is highly informative, because it allows us to follow how the positions at which the slider sticks change from cycle to cycle. Unfortunately, printed formats only allow for a few friction loops to be displayed.

However, many details of the friction loop shape can be conveyed by using an hexagonal bin plot [28, 29] as shown in figure 6. The graph shows the slider position x_{contact} on the vertical axis versus the number of elapsed cycles n_{cycles} on the horizontal axis.

The hexagonal bin plot is constructed in the following way. First, the graph area is divided into a honeycomb lattice of hexagonal bins, on top of which all 1.8 million measurement records of $\{n_{\text{cycles}}, x_{\text{contact}}, F_{\text{friction}}\}$ are scattered. For each bin, a single scalar value is now calculated from the data points inside it. This value determines the color of the bin. In principle it can be any metric that describes the data it contains, such as the mean, minimum, or maximum value, or even simply the value count. In this case, the bin color corresponds to the maximum value of F_{friction}. The plot can be understood as a collection of all measured friction loops 'viewed from the top'. It main strength is that it shows the evolution of the friction force magnitude and its distribution across the surface in a single plot.

In the first part of the experiment, in which 200 cycles were measured consecutively, there are three dominant stick

Table 2. Overview of all cycle numbers that mark a significant change in the experimental results. All of these cycle numbers are illustrated in the plots in this paper using colored dashed lines.

Line	Cycles	Event
- - - -	200	The experiment mode changes from slow to fast
- - - -	1700	Overall increase in stick force
- - - -	65 000	Start of overall smoothening of friction loops

locations, at 0 nm, 250 nm and 600 nm. During the first 10 cycles, the slider mostly sticks close to the last two locations, but from 20 cycles onwards the slider occasionally sticks at other locations as well. Immediately after the start of the second part of the experiment, in which fast, unmeasured cycles are executed between the measurements, the dominant stick locations are smoothened across the entire motion range. After 1700 cycles, the overall stick force suddenly increases across the entire surface. The force gradually decreases again until 65 000 cycles have elapsed and a new friction force maximum occurs. From this point onwards, the friction loops become very smooth and almost continuous.

We have marked the boundaries of the regions in our experiment in every graph in this paper using vertical dashed lines. Their meaning is summarized in table 2.

3.4. Stick–slip statistics

Slip events show up in the friction loops as discrete jumps, where the contact position increases more than the constant step size of the undisturbed motion. We automatically labelled pairs of data-records $\{p_n, p_{n+1}\}$ as stick–slip pairs when the following conditions were true simultaneously:

$$D \cdot (x_{\text{contact},n+1} - x_{\text{contact},n}) > 2 \cdot \Delta x_{\text{s,und}} \tag{15}$$

$$-D \cdot (F_{\text{contact},n+1} - F_{\text{contact},n}) > 2 \cdot k_{\text{s}} \cdot \Delta x_{\text{s,und}} \tag{16}$$

where $D = 1$ if the actuator voltage increases (forward sliding direction) and $D = -1$ if the actuator voltage decreases (backward sliding direction). $\Delta x_{\text{s,und}} = 0.74$ nm is the constant
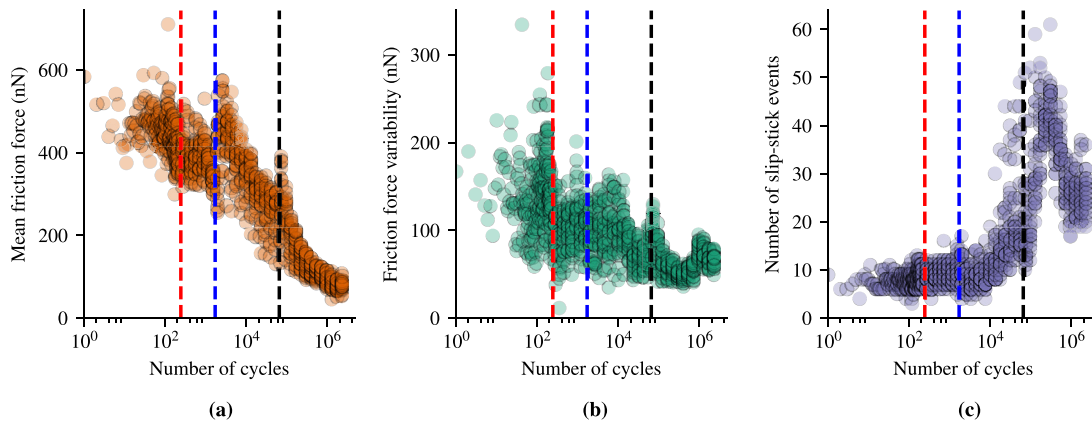
Figure 7. Scalar quantifiers obtained from the individual friction loops plotted versus the total number of elapsed cycles. (a) The mean friction force per cycle, (b) the standard deviation of the measured friction forces per cycle, and (c) the total number of slip events per cycle.

displacement step size as measured in the undisturbed motion curves. This allowed us to give each 'point of stick' (the continuous parts of the friction loops) and each stick–slip point pair (the arrows) a unique label, analyze their individual properties and study how their statistics develop as a function of the number of elapsed cycles.

When using a simple thresholding algorithm to detect steps in data, as we are doing here, the smallest detectable step is determined by the noise level of the data. In our case, the RMS displacement noise is an exceptionally low $\sigma_x = 0.2$ nm. As a rule of thumb, a safe detection threshold is often taken as $6\sigma = 1.2$ nm. This is less than twice the minimum displacement step of $2 \cdot \Delta x_{s,und} = 1.48$ nm that we are trying to detect, so our thresholding algorithm will yield reliable results for this dataset. For more noisy data this simple approach will not work and a more robust step detection algorithm should be used, such as the one discussed by Yao and Li [30].

The maximum absolute value of the lateral force at each point of stick is the static friction force at that specific location. Figure 7 shows the mean of the friction forces measured per cycle, their variability, and the total number of slip events in each measured cycle.

Figure 8 shows the evolution and spread of the coefficient of (static) friction $\mu_{f,s}$. Each data point is obtained by dividing the maximum lateral force before a slip occurs by the externally applied normal pushing force of $F_N = 669 \pm 51$ nN. During the first $\sim 10^5$ cycles, the mean coefficient of friction per cycle varied roughly in the range between the values of the static and dynamic coefficients-of-friction for glass–glass contacts of 0.94 and 0.4 respectively. After $\sim 10^5$ cycles the coefficient of friction decreased down to 0.12. The variability of the friction coefficient follows the same trend as the mean friction force shown in figure 7(b).

3.5. Semi-statically and dynamically dissipated energy

Our friction loops consist of two contributions: continuous 'stick parts', where the slider is stuck to the loader, and discontinuous 'slip parts', where the slider slips from one stick part to the next. When we calculate the dissipated energy from a friction loop, we have to treat these two contributions separately. We will refer to the energy dissipated while the slider
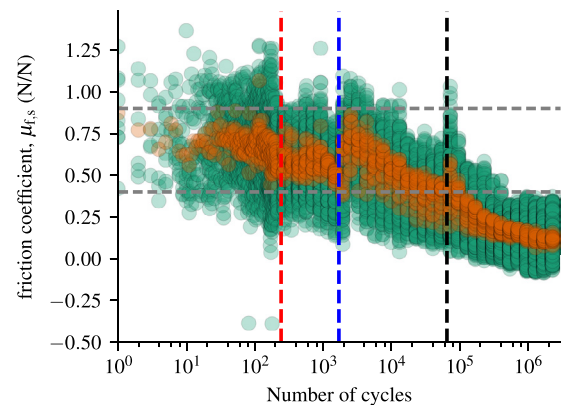
Figure 8. The coefficient of static friction: the maximum friction force before a slip occurred divided by the externally applied normal force. To provide a macro-scale frame of reference for the magnitude of these values, the horizontal dashed-light gray lines indicate the empirical values of the static (0.94) and dynamic (0.4) coefficients-of-friction for bulk glass–glass contacts [31].
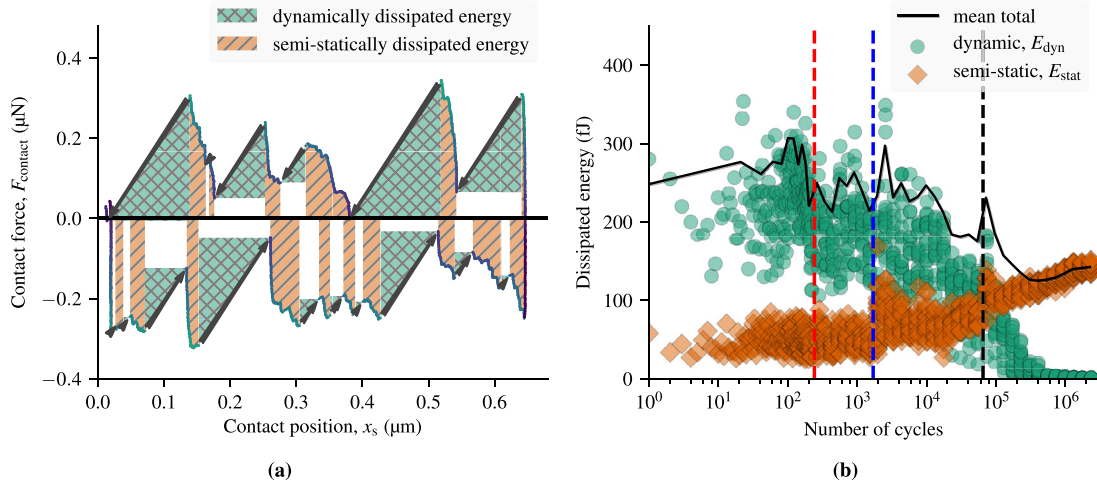
is stuck as the semi-statically dissipated energy, and to the energy dissipated during the slip events as the dynamically dissipated energy.

We choose the term 'semi-static' because it refers to the parts of the measurement where the slider is stationary and no inertia is involved. However, every dissipation process is inherently dynamic, not static, which is why we have added the 'semi'-prefix. The physical mechanisms by which semi-static dissipation occurs may involve, for example, small contact deformations and plastic yield of the contacting surfaces.

The term 'dynamic' refers to the fact that the underlying dissipation mechanisms are related to the dynamic behavior of the slider. While the slider is slipping, it may slide viscously and break weaker asperities along its path. When it finally gets stuck again, it will dissipate the remainder of its kinetic energy on impact.

The calculation of both energy contributions is illustrated in figure 9(a). We obtain the semi-statically dissipated energy by integrating $F_{friction}$ with respect to $x_{contact}$ between the start and end of a single stick part:

$$E_{static} = \int_{x_{start}}^{x_{end}} F_{friction} dx_{contact}, \qquad (17)$$

Figure 9. (a) Illustration of how the semi-statically dissipated energy and the dynamically dissipated energy are obtained from a friction loop. The semi-statically dissipated energy is the surface area below the continuous 'stick parts' of the friction loop. The dynamic energy is the surface area of the right-angled triangle defined by the slip arrows. This friction loop was recorded after 53 818 sliding cycles. It was selected because its semi-statically dissipated energy roughly equals its dynamically dissipated energy. (b) The dissipated energy versus the number of elapsed sliding cycles. The dynamic energy is the energy dissipated in slip motion events. The semi-statically dissipated energy is the energy dissipated while the loader is stuck but the contact yields somewhat. At low cycle numbers most energy is dissipated in the large slip events (see figure 5). At very high cycle numbers, the friction loops become very smooth, and almost all energy is dissipated semi-statically.

where E_{static} is the semi-statically dissipated energy.

The dynamically dissipated energy cannot be found by a similar integration method, because we do not have any position measurements during the slip motion itself. We only know where the slider starts slipping, and where it gets stuck again. However, the energy dissipated in a slip motion must be exactly equal to the decrease in potential energy stored in the slider support springs, regardless of exactly when and by which mechanism the energy is converted to heat. This means that we can calculate the energy dissipated in a single slip event from the difference between the spring energy E_{spring} just before and immediately after the slip motion:

$$E_{spring} = \frac{1}{2}kx^2 \tag{18}$$

$$\Delta E_{spring} = -\frac{1}{2}k\left(x_{before} - x_{after}\right)^2 \tag{19}$$

$$= -\frac{1}{2}k\Delta x^2 \tag{20}$$

$$E_{dynamic} = -\Delta E_{spring} = -\frac{1}{2}\Delta F_{contact}\Delta x_{contact}, \tag{21}$$

where $E_{dynamic}$ is the dynamically dissipated energy of the slip motion.

In our friction loops, equation (21) is equal to the surface area of the right-angled triangle defined by each slip motion arrow. These areas are shaded in green in figure 9(a). Note that this means that the total energy is not equal to the surface area of the friction loop, as is the case in an FFM-style friction loop (figure 3(b)).

Figure 9(b) shows the semi-statically dissipated energy and the dynamically dissipated energy of each cycle, as well as the mean of their sum, versus the total number of elapsed

cycles. In the first part of the experiment, most energy is dissipated dynamically, with a large variability. After the experimental mode is changed at 200 elapsed cycles, the dynamic energy decreases but the semi-static energy remains constant. After 1700 cycles, the dynamic part of the dissipated energy decreases, while the semi-static energy starts to increase monotonically. After 65 000 cycles, the dynamically dissipated energy quickly decreases to zero. The semi-static energy, however, keeps increasing monotonically until it finally starts to flatten off after 1 million cycles.

4. Discussion

Our visualizations of the individual friction loops in figure 6, the aggregated quantities shown in figure 7 and the dissipated energy together paint an indirect yet lively picture of the events that occurred at the contact.

4.1. Physical interpretation of the results

During the first part of the experiment the slider moves over the surface in several large jumps. The locations at which the slider sticks do not change much. After the experiment changes, high-speed sliding motions are executed between the measured cycles, and the surface changes instantly. This is because the inertia of the moving slider is now large enough to break the highest interlocking asperities, which has a noticeable effect on the magnitude of the friction force (figure 7(a)), the dynamically dissipated energy, and the friction coefficient. Because these surface changes happen during the fast cycles that are not measured, the surface remains relatively stable during the recorded measurement blocks where the slider inertia does not play a role and the available forces are not large enough to modify the contact significantly. This is

confirmed by a sharp decrease of the force variability (figure 7(b)) after the measurement type changes.

After 1700 cycles, the breakup of a large third body or asperity significantly increases the mean friction force and the friction coefficient, which causes a sharp increase in the amount of semi-statically dissipated energy. From this point onwards, the total number of slip events gradually increases while the friction force, friction coefficient and the dissipated energy decrease monotonically.

Around 65 000 cycles we observe the formation and destruction of an obstacle near the center of the sliding track, which is indicated by a peak in the mean friction force, the coefficient of friction, the force variability, and the total dissipated energy. A remarkable transition in friction behavior follows. The amount of slip events almost triples, yet the dynamically dissipated energy quickly drops to zero. The semi-statically dissipated energy, which had been rising steadily since the start of the experiment, becomes the dominant energy dissipation mode.

The friction loops are now almost completely smooth, which indicates that the previously dominant stick–slip behavior has changed to normal sliding. However, the shape of the friction loops has become highly asymmetric. For both directions of motion, the friction force gradually decreases when $x_{contact}$ is near the edge of the sliding track. In some cases it even becomes negative, indicating that at certain positions the slider is being dragged along rather than being held back. Our hypothesis for explaining this behavior is that a small amount of viscous slurry is formed at the contact, which consists of the pulverized remains of SiO_2 debris, carbon contaminants, and a small amount of adsorbed water. A small excess of the slurry at the far ends of the sliding track will pull on the slider by capillary action, which accounts for the observed negative friction forces. The excess of slurry increases capillary adhesion, which in turn increases the local static friction force. This accounts for the fact that the slider sticks at the far ends of the sliding track after the direction of motion is reversed. The slurry will also introduce some viscoelastic behavior along the length of the sliding track, and may in part be responsible for the smooth sliding behavior during the final stages of the experiment.

The steady rise of the semi-static energy after 1700 cycles may be caused by a gradual increase of the contact area due to flattening. This would increase the adhesion forces acting between the contacting surfaces, which in turn increases the friction force, as well as the amount of dissipated energy.

5. Conclusion

We have successfully measured the evolution of the static friction force between two contacting silicon MEMS sidewalls with a resolution of 0.6 nN. By compensating for the in-plane bending spring constant of the loader, we were able to obtain the friction force as a function of the real point of contact rather than the equivalent of the cantilever support position of an FFM measurement. This results in a more intuitive type of friction loop, because it does not require any knowledge of the measurement system with which the data was acquired.

Hexagonal bin plots are an effective visualization method for studying the evolution of the friction force in a reciprocating sliding motion as a function of any variable. Figure 6 gives a clear qualitative description of how the shape of the friction loop changes as a function of the total number of elapsed friction cycles.

The identification of individual slip events allowed us to split each friction loop into sections of stick and sections of slip, and we obtained two distinct mechanisms by which energy is dissipated. The semi-statically dissipated energy is related to the deformation of the contact by a variety of physical mechanisms before actual sliding occurs. The dynamically dissipated energy is related to the slider dynamics during the micro-scale slip motions and to the impact when the slider gets stuck again.

We have measured the variability and drift of the static friction coefficient (figure 8), the mean static friction force (figures 7(a) and (b)), and the number of slip events (figure 7(c)) as a function of the total number of elapsed cycles. The coefficient of friction is not an adequate metric by itself to describe the characteristics of friction in MEMS, because of its large variability with each friction cycle.

After a large number of sliding cycles the friction loop shapes remain the same. The semi-statically dissipated energy gradually increases throughout the experiment and levels off after 1 million cycles, indicating that the 'run-in' of the surfaces is complete. The dynamically dissipated energy is more variable than the semi-statically dissipated energy and decreases throughout the experiment, and eventually becomes zero when the stick–slip behavior of the contact has changed to continuous sliding.

The simultaneous existence of these two energy contributions in the same order of magnitude appears to be unique to the meso-scale, and to its characteristic multi-asperity contact. It would be of great value to study how these energies behave in meso-scale and atomic scale friction force microscopy measurements under well-controlled circumstances. The ability to disentangle the dissipated energy into two physically different contributions will enable more accurate conclusions to be drawn from all friction loop measurements.

Acknowledgments

ORCID iDs

Jaap Kokorian ⑩ https://orcid.org/0000-0001-9147-5869

References

[1] Bar-Sinai Y, Spatschek R, Brener E A and Bouchbinder E 2014 On the velocity-strengthening behavior of dry friction *J. Geophys. Res.: Solid Earth* **119** 1738–48

[2] Dieterich J H and Kilgore B D 1994 Direct observation of frictional contacts: New insights for state-dependent properties *Pure Appl. Geophys.* **143** 283–302

[3] Heslot F, Baumberger T, Perrin B, Caroli B and Caroli C 1994 Creep, stick-slip, and dry-friction dynamics: Experiments and a heuristic model *Phys. Rev.* E **49** 4973–88

[4] Rice J R and Ruina A L 1983 Stability of steady frictional slipping *J. Appl. Mech.* **50** 343

[5] Ruina A 1983 Slip instability and state variable friction laws *J. Geophys. Res.: Solid Earth* **88** 10359–70

[6] Mate C M, McClelland G M, Erlandsson R and Chiang S 1987 Atomic-scale friction of a tungsten tip on a graphite surface *Phys. Rev. Lett.* **59** 1942–5

[7] Dienwiebel M, Verhoeven G S, Pradeep N, Frenken J W M, Heimberg J A and Zandbergen H W 2004 Superlubricity of graphite *Phys. Rev. Lett.* **92** 126101

[8] Socoliuc A, Bennewitz R, Gnecco E and Meyer E 2004 Transition from stick-slip to continuous sliding in atomic friction: entering a new regime of ultralow friction *Phys. Rev. Lett.* **92** 134301

[9] Jinesh K B and Frenken J W M 2006 Capillary condensation in atomic scale friction: how water acts like a glue *Phys. Rev. Lett.* **96** 166103

[10] Prandtl L 1928 Ein Gedankenmodell zur kinetischen Theorie der festen Körpe *Z. Angew. Math. Mech.* **8** 85–106

[11] van Spengen W M 2015 A physical model to describe the distribution of adhesion strength in MEMS, or why one MEMS device sticks and another 'identical' one does not *J. Micromech. Microeng.* **25** 125012

[12] Maboudian R, Ashurst W R and Carraro C 2000 Self-assembled monolayers as anti-stiction coatings for MEMS: characteristics and recent developments *Sens. Actuators* A **82** 219–23

[13] Ashurst W R, Yau C, Carraro C, Lee C, Kluth G J, Howe R T and Maboudian R 2001 Alkene based monolayer films as anti-stiction coatings for polysilicon MEMS *Sens. Actuators* A **91** 239–48

[14] Buja F, Fiorentino G, Kokorian J and van Spengen W M 2015 Observation of nanoscale adhesion, friction and wear between ALD Al_2O_3 coated silicon MEMS sidewalls *Nanotechnology* **26** 255701

[15] Asay D B, Dugger M T and Kim S H 2008 *In-situ* vapor-phase lubrication of MEMS *Tribol. Lett.* **29** 67–74

[16] Mehregany M, Zorman C A, Rajan N and Wu C H 1998 Silicon carbide MEMS for harsh environments *Proc. IEEE* **86** 1594–609

[17] Buja F, Sumant A V, Kokorian J and van Spengen W M 2014 Electrically conducting ultrananocrystalline diamond for the development of a next generation of micro-actuators *Sens. Actuators* A **214** 259–66

[18] Wu J, Wang S and Miao J 2008 A MEMS device for studying the friction behavior of micromachined sidewall surfaces *J. Microelectromech. Syst.* **17** 921–33

[19] Ku I S Y, Reddyhoff T, Choo J H, Holmes A S and Spikes H A 2010 A novel tribometer for the measurement of friction in MEMS *Tribol. Int.* **43** 1087–90

[20] van Spengen W M and Frenken J W M 2007 The Leiden MEMS tribometer: real time dynamic friction loop measurements with an on-chip tribometer *Tribol. Lett.* **28** 149–56

[21] Luck D L, de Boer M P, Ashurst W R and Baker M S 2003 *Proc. 12th Int. Conf. on Solid-State Sensors, Actuators and Microsystems (Transducers)* vol 1 (IEEE) pp 404–7

[22] Elwenspoek M C 1993 On the mechanism of anisotropic etching of silicon *J. Electrochem. Soc.* **140** 2075–80

[23] Legtenberg R, Groeneveld A W and Elwenspoek M 1996 Comb-drive actuators for large displacements *J. Micromech. Microeng.* **6** 320

[24] van Spengen W M, Turq V and Frenken J W M 2010 The description of friction of silicon MEMS with surface roughness: virtues and limitations of a stochastic Prandtl–Tomlinson model and the simulation of vibration-induced friction reduction *Beilstein J. Nanotechnol.* **1** 163–71

[25] Kokorian J, Staufer U and van Spengen W M 2015 *Proc. 18th Int. Conf. on Solid-State Sensors, Actuators and Microsystems (Transducers)* pp 772–5

[26] Kokorian J, Buja F and van Spengen W M 2015 In-Plane displacement detection with picometer accuracy on a conventional microscope *J. Microelectromech. Syst.* **24** 618–25

[27] Hunter J D 2007 Matplotlib: a 2D graphics environment *Comput. Sci. Eng.* **9** 90–5

[28] Carr D B, Littlefield R J, Nicholson W L and Littlefield J S 1987 Scatterplot matrix techniques for large *N J. Am. Stat. Assoc.* **82** 424–36

[29] Hao M C, Dayal U, Sharma R K, Keim D A and Janetzko H 2010 Variable binned scatter plots *Inf. Vis.* **9** 194–203

[30] Yao Q and Li Q 2016 Line scan reconstruction: a viable approach for tracking atomic stick–slip events and true tip position in atomic force microscopy *Tribol. Lett.* **64** 31

[31] Haynes W M ed 2016 *CRC Handbook of Chemistry and Physics, Internet version* 96th edn (Boca Raton, FL: CRC Press) pp 15–48